

Initial growth of Ba on Ge(001): An STM and DFT studyW. Koczorowski,^{1,2,*} A. Puchalska,³ T. Grzela,² M. W. Radny,^{2,4} L. Jurczyszyn,³ S. R. Schofield,^{1,5}
R. Czajka,² and N. J. Curson^{1,6}¹*London Centre for Nanotechnology, University College London, 17-19 Gordon Street, London, United Kingdom*²*Institute of Physics, Poznan University of Technology, ul. Piotrowo 3, 60-965 Poznan, Poland*³*Institute of Experimental Physics, University of Wrocław, pl. Maksa Borna 9, 50-204 Wrocław, Poland*⁴*School of Mathematical and Physical Sciences, The University of Newcastle, Callaghan 2308, Newcastle, Australia*⁵*Department of Physics and Astronomy, UCL, London, WC1E 6BT, United Kingdom*⁶*Department of Electronic and Electrical Engineering, UCL, London, WC1E 7JE, United Kingdom*

(Received 20 February 2015; revised manuscript received 20 May 2015; published 29 June 2015)

An ordered alkaline-earth submonolayer on a clean Si(001) surface provides a template for growth of the atomically sharp, crystalline Si-oxide interface that is ubiquitous in the semiconductor device industry. It has been suggested that submonolayers of Sr or Ba on Ge(001) could play a similar role as on structurally identical Si(001), overcoming known limitations of the Ge(001) substrate such as amorphization of its oxidation layers. In this paper the initial stage of the Ba oxidation process, i.e., adsorption and organization of Ba atoms on the Ge(001) surface as a function of temperature (270–770 K) for coverage 1.0 monolayer (ML) and 0.15–0.4 ML, is studied using scanning tunneling microscopy (STM) and density functional theory (DFT). Three types of features have been identified on the Ba-covered Ge(001) surface. They originate from isolated Ba adatoms, isolated Ba ad-dimers, and the Ba ad-dimers assembled into short-range, randomly distributed chains that run across the Ge dimer rows. We find from both STM measurements and DFT calculations that the latter is the dominant structure on Ge(001) with increasing coverage.

DOI: [10.1103/PhysRevB.91.235319](https://doi.org/10.1103/PhysRevB.91.235319)

PACS number(s): 68.35.bg, 68.37.Ef, 68.55.A–, 73.40.Vz

I. INTRODUCTION

Silicon (Si) continues to dominate advanced semiconductor integrated circuit technologies, but further miniaturization and developments of Si-based devices become problematic as they approach both technological and fundamental limits. Intensive research has been conducted to integrate alternative semiconductor materials into the Si mainstream complementary metal-oxide-semiconductor (CMOS) platform to add new functions, but also to preserve compatibility with existing technology. The latter creates a growing interest in germanium (Ge), and especially in the Ge(001) surface, which is structurally identical to the Si(001) substrate. It is known, however, that depositing the same elements on Si(001) and Ge(001) does not usually cause analogous behavior and structure formation, indicating important differences in surface chemistry and energetics of the two materials [1–4]. Among specific integration challenges, such as doping control or low-resistance contact formation, the ability to grow a high-quality, epitaxial-ordered, alkaline-earth submonolayer on Ge(001), which is equivalent to effective crystalline oxide gate epitaxy on Si(001), remains of critical importance.

Beyond this, the issue of complex oxide growth on Si and Ge has current and broad-reaching scientific and technological importance. The fabrication of thin-film complex oxides enable exploration of fundamental processes such as piezo and ferroelectric polarization [5,6], carrier density modulation in semiconductors due to ferroelectric switching [7,8], strong electro-optic activity [9], and giant tunneling electroresistance [10]. Through the understanding of these

processes, technologies such as nonvolatile memories and low-power devices are expected to emerge [7,11].

The epitaxial growth of complex oxides on Si(001) requires careful control and preparation of the substrate. The established method begins with depositing up to 0.5 monolayers (ML) of an alkaline-earth metal (usually Sr or Ba), which passivates the surface against the creation of amorphous silicates, such as SiO₂, and provides an ordered template layer for the crystalline, atomically sharp Si-oxide interface formation [12–14].

In general, depending on the deposition temperature, there are two experimentally verified paths for creating the appropriate template on Si(001) [15,16]. At low temperatures (270–670 K) the motion of Si surface atoms is kinetically hindered and the deposition leads to the on-surface adsorption of the Sr or Ba adatoms. This process retains the initial (2 × 1) symmetry of Si(001) up to 0.5 ML. At temperatures between 670 and 970 K, a new ordered (3 × 2) phase is formed at 1/6 ML, followed by the (2 × 1) reconstruction at 0.5 ML and the (3 × 1) phase near 1.0 ML. The phases on annealed Si(001) are predicted to be formed due to reorganization of the Si surface atoms and the formation of surface alloys [15,16].

There are very few matching reports for the Ge(001) surface. An atomically clean BaTiO₃/BaGe₂/Ge interface formation was reported by McKee *et al.* [17], suggesting that Ba termination of the Ge surface exhibits a similar effect as Sr or Ba on Si. Cattoni *et al.* [18] studied the effect of Ba overlayers on the chemical passivation of Ge(001) using low-energy electron diffraction (LEED), ultraviolet photoemission spectroscopy (UPS), and x-ray photoemission spectroscopy (XPS). They concluded that at coverages of 1.2 and 1.5 ML, the order of Ba on Ge(001) is different to that observed for Sr on Si(001), and that the presence of Ba on the Ge(001) surface at the reported experimental

*Corresponding author: wojciech.koczorowski@put.poznan.pl

conditions increases its oxidation tendency. Recently Lukanov *et al.* [19–21] observed, using scanning tunneling microscopy (STM), a series of ordered (3×4) , (3×2) , (9×1) , and (6×1) phases on the Ge(001) surface dosed with Sr at 675 K and annealed subsequently at 900 K. Their detailed analysis of the $(3 \times 4) - 1/6$ ML structure lead them to adopt the $(3 \times 2) - 1/6$ ML double-dimer vacancy alloy model developed for Sr-Si(001) to the Sr-Ge(001) system [20]. Some structures induced by the Ba atoms on annealed Ge(001) were also observed, however, without atomic resolution [19]. Recently we presented STM observations on surface morphology and structural evolutions of Ba at 1.0 ML on the Ge(001) substrate induced by postdeposition thermal processing [22].

In this paper we present a detailed experimental STM and computational density functional theory (DFT) study of the adsorption of Ba on the Ge(001) surface as a function of temperature and coverage. We show, using atomic resolution STM analyses, that adsorption of the Ba atoms on the Ge(001) leads to formation of the short-range ordered, linear chains on the surface for coverage up to about 0.4 ML. Higher Ba coverage (1 ML) evolves from the disordered phase (after deposition at room temperature) to the short-range ordered phase (~ 570 K). Long-range ordered phases of Ba on Ge(001) were not detected in any of the studies we performed. The DFT calculations reveal that a simple Ba adatom model adequately describes the three common features identified on the Ba-covered Ge(001) surface—adsorbed isolated Ba adatoms, isolated Ba dimers, and chains that consist of the Ba dimers. The calculations of the surface free energy as a function of coverage indicate that the disordered chains should be preferred under Ba-rich conditions, which also agrees with experiment.

II. METHODOLOGY

A. Experimental

The STM measurements were performed in ultrahigh vacuum (UHV) with the base pressure below 1×10^{-10} mbar using the variable-temperature (VT) STM Omicron XA unit head. All surface preparation and modifications were completed in a UHV-connected preparation chamber with the base pressure below 5×10^{-10} mbar.

The Ge substrates were cut from an *n*-type Sb-doped wafer with resistivity of $1 \sim 10 \Omega \text{ m}$. The clean Ge(001) $c(4 \times 2)$ was prepared by a few cycles of Ar⁺ ion sputtering at 0.75 keV (at a partial pressure of Ar of 1×10^{-5} mbar) followed by annealing at 970 K at UHV by direct heating method. The Ba atoms were evaporated using a commercial Omicron EFM-3 evaporator with a Mo crucible (electron energy 500 V, 10-nA flux current), preceded a by long (>100 h), continuous degas to reduce pressure to 1×10^{-9} mbar during evaporation.

Three different temperature and coverage deposition regimes were examined. The first sample was prepared by evaporating 1.0 ML of Ba on Ge(001) at room temperature (RT), followed by the subsequent annealing at 470, 570, 670, and 770 K (for 30 min). The second sample was prepared by evaporation of 0.4 ML of Ba on Ge substrate at RT. The third sample was prepared by evaporation of 0.15 ML of Ba at RT. The STM images were taken at 100 K and RT using the

electrochemically etched tungsten tips. The data processing was carried out using the WSXM software [23].

B. Computational

Spin-polarized DFT calculations were performed using plane waves, projector-augmented wave (PAW) potentials [24], the generalized gradient approximation (GGA) for exchange and correlation [25], and the energy cutoffs for the PAW potentials as implemented in the VASP code [26,27]. Ba atoms were adsorbed on the Ge(001) $c(4 \times 2)$ surface represented by an asymmetric slab (with the calculated bulk lattice constant of 5.78 Å) containing six layers within a 4×4 surface unit cell with the bottom surface of the slab terminated by hydrogen atoms. In the total energy calculations the top five layers were allowed to move. Four special **k** points in the irreducible symmetry element of the surface Brillouin zone and energy convergence tolerance of 10^{-7} eV were also used.

The surface charge and probability densities were calculated by integrating the local density of states function (ILDOS) over an energy range of ± 1.0 and ± 2.0 eV from the Fermi energy (E_F). The obtained data are presented as xyz plots in which the height z is associated with tracing out a selected ILDOS isosurface value and then converted into a grayscale. Such representations of the calculated densities can be interpreted as bias-dependent simulated STM images of a surface within the Tersoff-Hamann approximation [28].

The relative energetics of the various Ba structures formed on Ge(001) were analyzed using the method of *ab initio* atomistic thermodynamics [29,30], where the availability of the Ba adatoms from the environment in thermal equilibrium is represented by the Ba chemical potential. For a given chemical potential of the Ba adatoms, the thermodynamically preferred surface is the one with the lowest surface free energy calculated from

$$\gamma = \frac{1}{A} [E_{\text{Ba/Slab}} - E_{\text{Clean-Slab}} - N_{\text{Ba}} \mu_{\text{Ba}}], \quad (1)$$

where γ is the surface free energy per unit surface area relative to the Ba-free Ge(001) $c(4 \times 2)$ reconstructed surface, N_{Ba} is the number of Ba adatoms with chemical potential μ_{Ba} , and $E_{\text{Clean-Slab}}$ and $E_{\text{Ba/Slab}}$ are the DFT total energies of the clean slab and the slab with the adsorbed Ba adatoms, respectively. Defining

$$\Delta \mu_{\text{Ba}} = \mu_{\text{Ba}} - E_{\text{Ba}}, \quad (2)$$

where E_{Ba} is the energy of a free Ba atom, Eq. (1) can be rewritten as

$$\gamma = \frac{1}{A} [E_{\text{Ba/Slab}} - E_{\text{Clean-Slab}} - N_{\text{Ba}} E_{\text{Ba}} - N_{\text{Ba}} \Delta \mu_{\text{Ba}}]. \quad (3)$$

In these expressions the vibrational, entropy, and pressure volume terms are ignored, as all of them are expected to be small [30].

III. RESULTS AND DISCUSSION

A. Clean Ge(001)

Figure 1 shows the filled [Fig. 1(a)] and empty [Fig. 1(b)] states experimental and simulated STM images of the clean

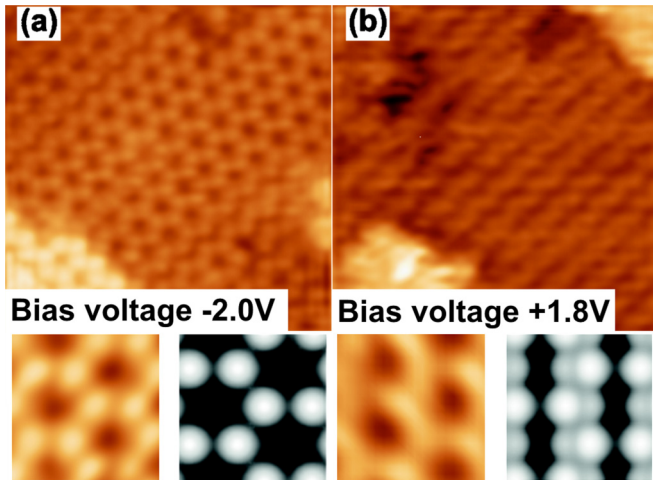


FIG. 1. (Color online) Filled-state (a) and empty-state (b) experimental (imaged at 100 K) and simulated STM images. The experimental images: $10 \times 10 \text{ nm}^2$, $I = 1 \text{ nA}$, $U = -2.0 \text{ V}$ and 1.8 V , respectively. Insets: (a) $2 \times 2 \text{ nm}^2$, $I = 1 \text{ nA}$, $U = -2 \text{ V}$ and (b) $2 \times 2 \text{ nm}^2$, $I = 20 \text{ pA}$, $U = 2 \text{ V}$. The simulated images (black-and-white insets) were obtained within the Tersoff-Hamann approximation, the simulations using a 4×4 surface unit cell with integration of the LDOS over $\pm 1.0 \text{ eV}$ from the Fermi energy and isosurface value of $2.35 \times 10^{-4} e/\text{\AA}^3$.

Ge(001) surface. The ground state of clean Ge(001) consists of the alternatively buckled Ge dimers in the $[110]$ and $[1\bar{1}0]$ directions, resulting in the $c(4 \times 2)$ reconstruction at low temperatures (below 200 K (e.g., Ref. [2])). The dimer rows are arranged in the $[1\bar{1}0]$ direction. The surface charge is accumulated on the double-occupied dangling-bond orbitals of the up-buckled Ge dimer atoms. In the filled-state imaging [Fig. 1(a)] the occupied surface electronic states are sampled and the bright protrusions are centered on the up-buckled Ge dimer atoms (see, for example, Ref. [2]). The dangling-bond orbitals on the down Ge dimer atoms are empty and tend to accept electrons. Therefore they are imaged dark in the filled-state images but are bright in the empty-state images [Fig. 1(b)].

B. Ba-covered Ge(001)– Experiment

Figure 2 shows a sequence of the STM images of the Ge(001) surface deposited with 1.0 ML of Ba atoms at room temperature (RT) [Fig. 2(a)] and subsequently annealed at 470 K [Fig. 2(b)], 570 K [Fig. 2(c)], 670 K [Fig. 2(d)], and 770 K [Fig. 2(e)].

After deposition of 1.0 ML of Ba on the Ge(001) surface at RT and initial annealing at 470 K, the Ba layer is seen to be in a disordered fashion, i.e., no ordered structures were observed [see Figs. 2(a) and 2(b)]. After annealing at 570 K [Fig. 2(c)], the short-range, linear (chains) structures of Ba develop. This ordering process continues and completes after annealing the sample at 670 K [Fig. 2(d)] and 770 K [Fig. 2(e)], respectively. We note that the observed linear assembly of adsorbates is correlated with an apparent reduction of the Ba coverage, which we interpret as being due to thermal desorption of the Ba adatoms (compare Figs. 2(a) and 2(e) [22]). Similar linear Ba

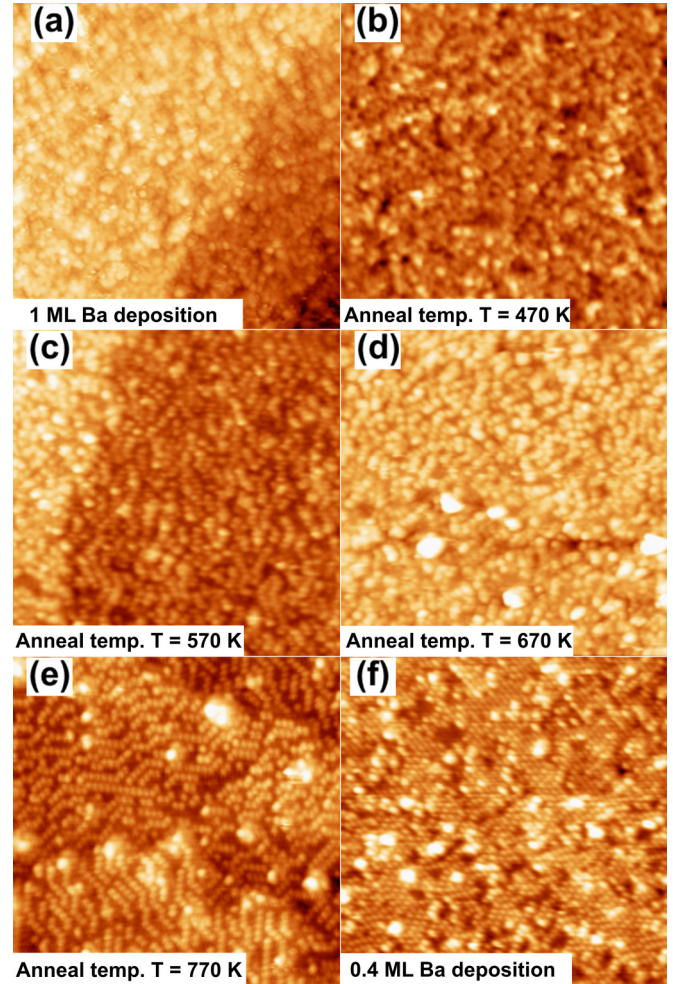


FIG. 2. (Color online) Ba structures formed after deposition of 1.0 ML on the Ge(001) substrate (a) at RT ($I = 40 \text{ pA}$, $U = -2 \text{ V}$), and after subsequent annealing at (b) 470 K ($I = 80 \text{ pA}$, $U = -2 \text{ V}$), (c) 570 K ($I = 120 \text{ pA}$, $U = 2 \text{ V}$), (d) 670 K ($I = 30 \text{ pA}$, $U = 2 \text{ V}$), (e) 770 K ($I = 120 \text{ pA}$, $U = 2 \text{ V}$), and (f) after deposition of 0.4 ML of Ba on Ge(001) at RT ($I = 200 \text{ pA}$, $U = 2 \text{ V}$). Images size $50 \times 50 \text{ nm}^2$.

structures were observed after evaporation of 0.4 and 0.15 ML of Ba on the Ge(001) substrate kept at RT, shown in Fig. 2(f) and Fig. 3, respectively.

Close inspection of the large-scale STM image in Fig. 3(a) and its zoomed-in area in Fig. 3(b) reveals a number of coexisting features that are typical for the investigated Ba/Ge(001) system but are not clearly seen on the Ba/Ge(001) surface at higher coverages.

First, the adsorption of Ba leads to the Ge surface dimers being buckled and results in a $c(4 \times 2)$ surface reconstruction at room temperature. The apparent height of protrusions attributed to the Ba-induced adsorbed structures changes as a function of applied sample bias. Imaging at negative-bias voltage (filled-state images) shows that the apparent height of the features decreases from $\sim 0.12 \text{ nm}$ at -2 V to $\sim 0.04 \text{ nm}$ at -1 V , while at positive bias voltage the apparent height of the features increases from $\sim 0.08 \text{ nm}$ at 2 V to $\sim 0.12 \text{ nm}$ at 1 V . Also, the empty-state STM images have better

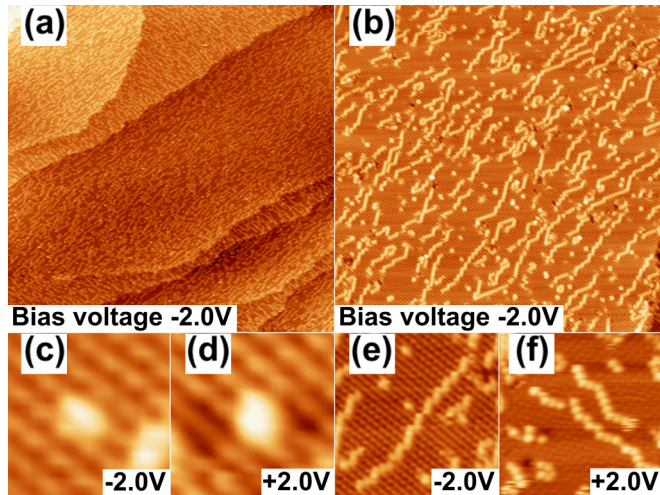


FIG. 3. (Color online) (a) Typical large-scale ($400 \times 400 \text{ nm}^2$) filled-state STM image of the Ge(001) surface covered with Ba 0.15 ML, deposited at room temperature ($I = 20 \text{ pA}$, $U = -2 \text{ V}$); (b) magnified section of Fig. (a) ($100 \times 100 \text{ nm}^2$); (c) asymmetric and (d) symmetric isolated features ($5 \times 5 \text{ nm}^2$, $I = 160 \text{ pA}$, $U = -2 \text{ V}$); (e) filled- and (f) empty-state images of a chain ($20 \times 20 \text{ nm}^2$, $I = 160 \text{ pA}$, $U = \pm 2 \text{ V}$).

resolution with ball-shaped protrusions clearly visible. Rather blurred protrusions are observed in the filled-state STM images.

Second, one observes that short-range chains are formed on the surface at different locations on the terraces with no preference for assembly along or across the step edges. This is somewhat surprising, as the step edges are expected to be the most reactive sites on the surface.

Third, the linear and/or zigzag, randomly distributed chains run across the Ge dimer rows in the $[310]$, $[110]$ and/or $[1\bar{1}0]$ directions [see Figs. 3(e) and 3(f)]. It should be noted that the adsorption of Ba adatoms does not induce any new buckling arrangement of the Ge dimers, i.e., the arrangement is the same as on the clean Ge(001) $c(4 \times 2)$ reconstructed surface.

Finally, we have also identified two other, less common, features on Ba-covered Ge(001)—an isolated, asymmetric bright protrusion on one side of the Ge dimer row [Fig. 3(c)] and an isolated, symmetric bright protrusion centered between two adjacent Ge dimer rows [Fig. 3(d)].

We note that the Ba chains follow the same directions as Ge dimers deposited onto Ge(001) at modest temperatures [31]. We believe, however, that different mechanisms are responsible for the observed similarity. The direction of the Ba dimers and the chains on Ge(001) are determined by the predominantly ionic type of interaction between the Ba adatoms and the Ge(001) substrate, as discussed later in this paper. This interaction leads to the formation of the Ba dimers in the valley bridge configuration, where each atom of the dimer is located in a separate hollow site on Ge(001). As a result there is no direct covalent bond between the Ba atoms in the dimer. This is in contrast to the Ge dimer deposited on Ge(001), which consists of a pair of Ge atoms located at the single hollow site with the covalent bond between the Ge atoms.

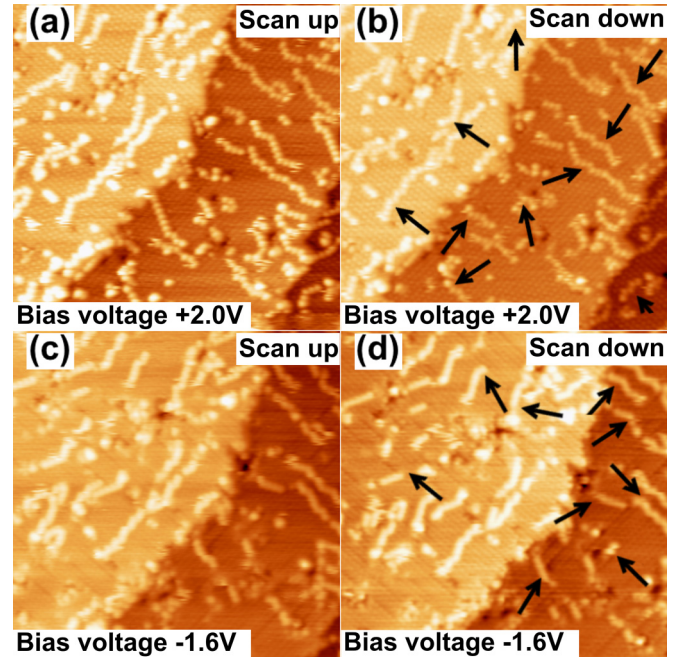


FIG. 4. (Color online) (a, b) Empty- ($+2 \text{ V}$, $I = 20 \text{ pA}$) and (c, d) filled- (-1.6 V , $I = 20 \text{ pA}$) state STM images of the same surface ($50 \times 50 \text{ nm}^2$), scanned from bottom to top (a, c) and top to bottom (b, d). Some chains are observed to be rearranged on the surface after scanning. Black arrows in (b) and (d) highlight parts of the dimer chains which have been seen to be mobile (with respect to (a) and (c), respectively) due to the STM tip influence.

Finally, while the high density of Ba adatoms on the Ge(001) surface [such as in Figs. 2(e) and 2(f)] stabilizes the chain positions, parts of the chains formed at lower coverage (Fig. 3) were observed to move during scanning. Figure 4 illustrates the chains rearranged on the Ge(001) surface by the STM tip during scanning the sample at both bias polarization and in both directions, from bottom to top or vice versa, at the fixed bias voltage. The data in Fig. 4 indicates that at low coverage (0.15 ML) coverage the Ba chains are weakly bonded to the Ge(001) substrate. STM-tip-enhanced diffusion is a commonly observed effect (e.g., Refs. [32] and [33]), usually attributed to the presence of the strong electric field intensity that is naturally created when a sample-tip bias of the order of $\pm 1 \text{ V}$ is applied across a tunnel junction which is $< 1 \text{ nm}$ in physical separation. This local electric field highly modifies the charge distribution in the vicinity of the Ba adatom occupied adsorption site. As a consequence the barrier height for diffusion of the ad-dimer can be reduced and its motion across the surface encouraged.

In summary, the observations reported in this section suggest that the observed Ba adatom-induced features on Ge(001) result from the on-top type of adsorption of the Ba atoms on Ge(001). The Ba chains are stabilized by the interaction with the Ge dimers without any rebonding of Ge surface atoms. Also, the higher the density of the Ba chains on Ge(001), the more stable the Ba adatom structures. In the next section some clarification of the nature of the observed features will be presented based on DFT calculations.

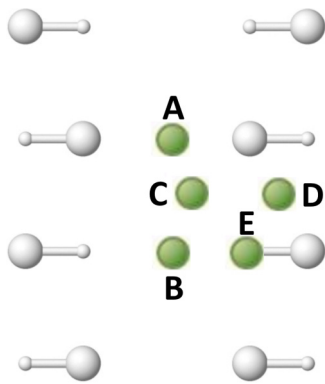


FIG. 5. (Color online) Schematics of the initial atomic structures of Ba/Ge(001) with a single Ba atom per 4×4 unit cell (1/16-ML coverage). The large and small white spheres denote the up and down Ge dimer atoms, respectively. Green spheres denote Ba adatoms.

C. Ba-covered Ge(001)– Modeling

In a search for the most likely atomic configurations of the adsorbed Ge(001) substrate, we have studied a large number of structures that we believe represent the most plausible configurations for the experimentally observed features (21 distinct structures in total have been analyzed). For the most energetically stable configurations we have simulated the STM images to compare with the experimentally observed features.

For one Ba adatom per 4×4 surface unit cell of Ge(001) $c(4 \times 2)$, which corresponds to the coverage of 1/16 ML, we have considered five adsorption sites: two inter-row bridge sites (sites A and B in Fig. 5), the end-dimer

bridge (site C in Fig. 5), intrarow (D in Fig. 5), and dimer end site (E in Fig. 5).

For two Ba adatoms per 4×4 unit cell (1/8-ML coverage), the considered structures are shown in Fig. 6. Due to the periodic boundary conditions imposed on the 4×4 unit cell, the first four configurations represent infinite zigzaglike atomic chains at different positions relative to the Ge(001) substrate [Figs. 6(a)–6(d)]. The configurations of Figs. 6(e)–6(g) and Figs. 6(h) and 6(i) represent atomic chains that run across and along the Ge dimer rows, respectively. The structures in Figs. 6(j) and 6(k) show two Ba dimers (per 4×4 unit cell) located in the trench between the adjacent Ge dimer rows and on top of the Ge dimer row, respectively.

Configurations considered for the four Ba adatoms per 4×4 unit cell (coverage of 0.25 ML) are shown in Fig. 7. All of them represent the Ba chains on Ge(001), with a Ba dimer of Fig. 6(k) as a repeating motif.

Table I provides an overview of the calculated adsorption energies (per Ba adatom) for all stable structures. Figure 8 illustrates the topology of the most stable configurations for each considered coverage.

The data shows that the most stable configuration for a single Ba atom per 4×4 unit cell (1/16 ML) is the end-dimer bridge structure [site C in Fig. 5; for structural details see Fig. 8(a)]. The structure with the Ba adatom located centrally in the trench between the Ge dimer rows (site B in Fig. 5) is by 0.08 eV higher in energy. In this configuration only one Ge dimer [labeled 4 in Fig. 8(a)] is significantly affected by the Ba adatom; its buckling angle is reduced from 19.6° to 3.8° , and its dimer bond length increases from 2.58 to 2.70 Å. These structural changes suggest that two 6s electrons of the Ba atom are donated into an unoccupied dangling-bond orbital

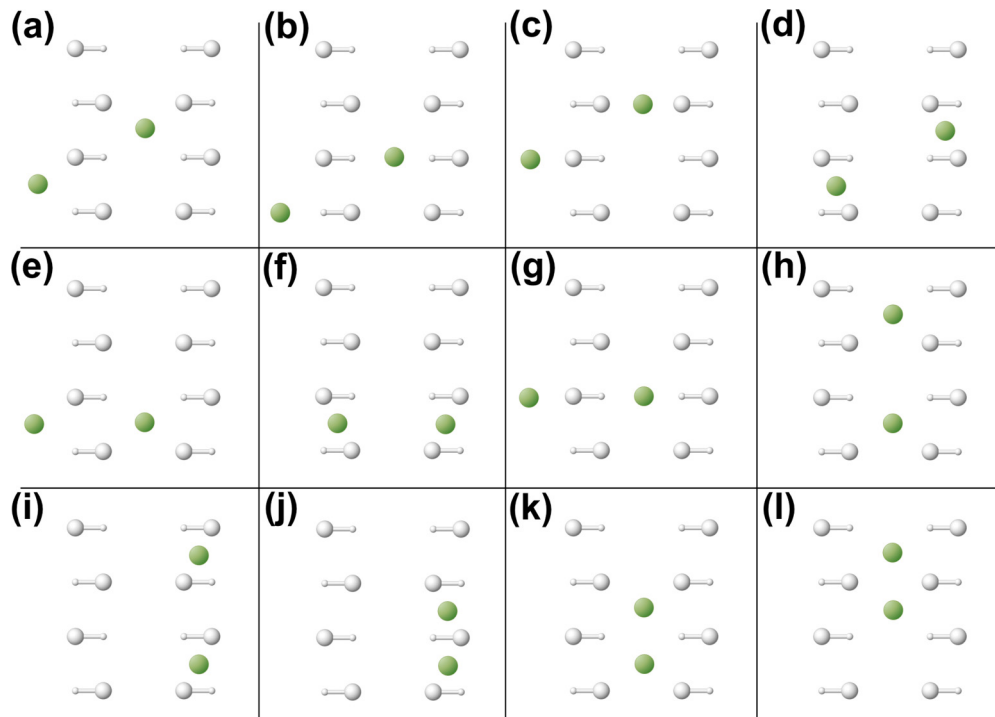


FIG. 6. (Color online) Schematics of initial configurations of Ba/Ge(001) with two Ba atom per 4×4 unit cell (1/8-ML coverage). The large and small white spheres denote up and down Ge dimer atoms, respectively. Green spheres denote Ba adatoms.

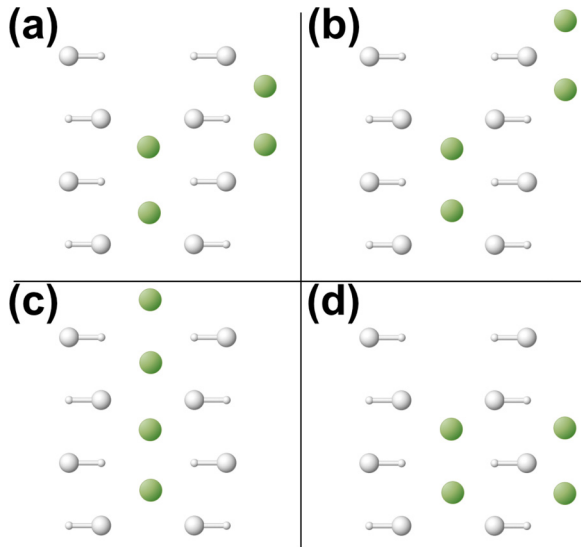


FIG. 7. (Color online) Considered initial configurations of Ba/Ge(001) with four Ba atoms per 4×4 unit cell (1/4-ML coverage). The large and small white spheres denote up and down Ge dimer atoms, respectively. Green spheres denote Ba adatoms.

of the Ge dimer [labeled 4 in Fig. 8(a)], resulting in the dimer being flattened and the dimer bond length elongated. The effect of such charge transformation is clearly seen in the simulated STM images presented in Fig. 9. Pink and blue arrows indicate equivalent Ge dimer rows in the STM and simulated images in Fig. 9. The filled-state STM image of Fig. 9(a) has one additional bright protrusion (pink arrow) compared to the corresponding image of clean Ge(001) [see Fig. 1(b)], which originates from the empty dangling-bond orbital of the Ge down-dimer atom filled by the electrons from the Ba adatom. Consequently, the site on the surface where the Ba adatom adsorbs is imaged dark in the filled state, meaning that there is no charge on the Ba adatom. However,

TABLE I. Adsorption energies (per adatom) of Ba on Ge(001) for all stable structures shown in Figs. 5–7. The energies of the most stable configurations are in bold.

| | E_{ad} [eV] | | |
|-------------|--|--|--|
| | 1 Ba adatom per unit cell (1/16 ML) Fig. 5 | 2 Ba adatoms per unit cell (1/8 ML) Fig. 6 | 4 Ba adatoms per unit cell (1/4 ML) Fig. 7 |
| Config. (a) | 3.56 | 3.95 | 4.15 |
| Config. (b) | 3.70 | 3.69 | 4.14 |
| Config. (c) | 3.78 | 3.33 | 3.93 |
| Config. (d) | 3.60 | 3.57 | 3.96 |
| Config. (e) | 2.79 | 3.68 | - |
| Config. (f) | - | 3.54 | - |
| Config. (g) | - | 3.97 | - |
| Config. (h) | - | 3.74 | - |
| Config. (i) | - | 3.56 | - |
| Config. (j) | - | 3.55 | - |
| Config. (k) | - | 4.15 | - |
| Config. (l) | - | 3.67 | - |

the Ba adatom can be seen in the empty-state image at higher bias (integration range of +2.0 eV in the simulated image 9(f) between blue and pink arrows) as a bright, circular protrusion located in the trench between the Ge dimer rows. At lower bias (integration range +1.0 eV) the Ba adatom is not visible and the image is very similar to that of the clean surface [compare Figs. 9(b) and 9(e) (+1.0 eV)]. We conclude, therefore, that the character of the bonding in the Ba/Ge system is strongly ionic, and the positively charged Ba ion is stabilized on the surface by electrostatic interaction with three negatively charged Ge dangling bonds. The simulated and experimental filled-state images match very well [compare Figs. 3(c), 9(a), and 9(d) (-1.0 eV)]. Also, the shape, distribution, and intensity of the protrusions in Fig. 9(d) (-1.0 eV) were found to be independent of the LDOS integration range.

The adsorption of two Ba atoms per 4×4 unit cell (coverage of 1/8 ML) leads to the formation of a Ba dimer as the most stable configuration [see Fig. 6(k)]. The structural parameters of the modified surface presented in Fig. 8(b) show that the Ba adatoms are located in the valley bridge configuration, where each atom of the dimer is located in a separate hollow site, forming a Ba atom pair aligned along the valley of the [1-10] surface direction. There is no direct covalent bond between the Ba atoms in the dimer.

We also observe that in this case two Ge dimers [2 and 4 in Fig. 8(b)] on the two adjacent dimer rows are significantly affected by the Ba adatoms—their buckling angles are reduced from 19.6° to 5.2° , and the dimer bond lengths increase from 2.58 to 2.73 Å.

Figure 10 shows the corresponding simulated STM images calculated for different values of the LDOS integration range. We observe that in the filled-state images there are two additional bright protrusions and both correspond to the originally empty dangling-bond orbitals of the Ge dimer down atoms [dimers 2 and 4 in Fig. 8(b)] filled by two pairs of 6s electrons from the two Ba adatoms [see the center region labeled by the red hexagon in Figs. 10(a) and 10(c)]. The Ba adatoms can only be identified in the empty-state images as a white protrusion of elliptical shape [see Fig. 10(d) (+2.0 eV)]. Such behavior suggests strong ionic character in the bonding system. It follows that the increased stability of the Ba dimer (adsorption energy of 4.15 eV) compared with that calculated for the isolated Ba atom (adsorption energy of 3.78 eV) results from an increased number of the filled dangling bonds on the Ge surface atoms surrounding each Ba ad-dimer ion. The simulated filled-state STM image matches well the experimental one shown in Fig. 3(d).

The details of the geometry of the most energetically favorable configuration with four Ba atoms per 4×4 unit cell (1/4 ML) of Fig. 7(a) are shown in Fig. 8(c). In this structure the four Ba adatoms form the zigzag-chainlike structure on the extended surface that consists of the Ba dimers. We observe that four Ge dimers (1, 2, 3, and 4) on the two adjacent Ge dimer rows are affected by the four Ba adatoms—their buckling angles are reduced from 19.6° to 2.6° , and the dimer bond lengths increase from 2.58 Å to 2.69 Å.

In Fig. 11 the simulated STM images of the most stable zigzag chain configuration of Fig. 7(a) are shown. One observes that the characteristic motifs seen in the simulated filled- and empty-state STM images for an isolated Ba dimer

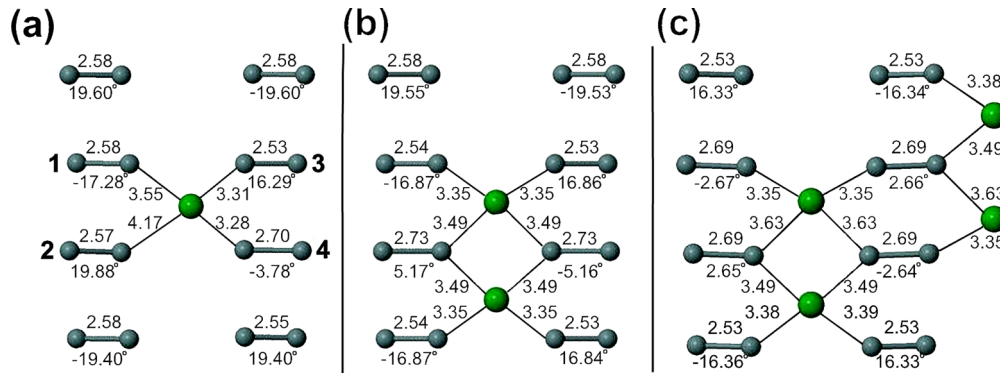


FIG. 8. (Color online) Top views of the most stable structures of Ba/Ge(001) with (a) one (1/16 ML), (b) two (1/8 ML), and (c) four (1/4 ML) Ba adatoms per 4×4 unit cell. The structural parameters are also shown. The Ba-Ge bond lengths (indicated by the lines between Ba and Ge atoms) are in angstroms and the dimer buckling angles are in degrees. A positive sign of the latter indicates that the dimer atom on the left is higher than the one on the right. Only first layer Ge atoms are shown.

(Fig. 10) are clearly reproduced here. It follows that the chains of Fig. 11 that consist of the Ba dimers are stabilized by electrostatic attraction between an optimally balanced number (and distribution) of negatively charged, six Ge dangling bonds and positively charged (two) Ba ad-dimers. The simulated images match very well the chain structure shown in Figs. 3(e)–3(f), 11(e), and 11(f).

The data in Table I shows that there are quite small adsorption energy differences between the most stable structure at 1/8 ML and two stable structures at 0.25 ML (4.14 and 4.15 eV, respectively). For this reason we have performed thermodynamic analysis of the energetics of the stable configurations under equilibrium Ba-rich and Ba-lean conditions. In this approach the thermodynamic potential of the surface is represented by the Gibbs free energy as a function of the

chemical potential of the adsorbed species (for details see, for example, [34]). The results of the calculations are shown in Fig. 12.

The data shows that under Ba-rich conditions (small negative Ba chemical potential) the zigzag chains composed of the Ba dimers [Figs. 7(a) and 7(b)] are clearly preferred. In the most stable zigzag chain of Fig. 7(a), every second Ba dimer is displaced along the trench between the Ge dimer row by half of the surface lattice constant, while in the second-lowest energy zigzag chain of Fig. 7(b), every second Ba dimer is displaced by one surface lattice constant. The small energy difference between these configurations (~ 0.01 eV) indicates that the positions of the Ba dimers in the trenches between the Ge dimer rows are weakly correlated, and the chains of different arrangement of the Ba dimers across the substrate Ge dimer rows may coexist on Ge(001), except those shown in Figs. 7(c) and 7(d). This can lead to the formation of short-range ordered,

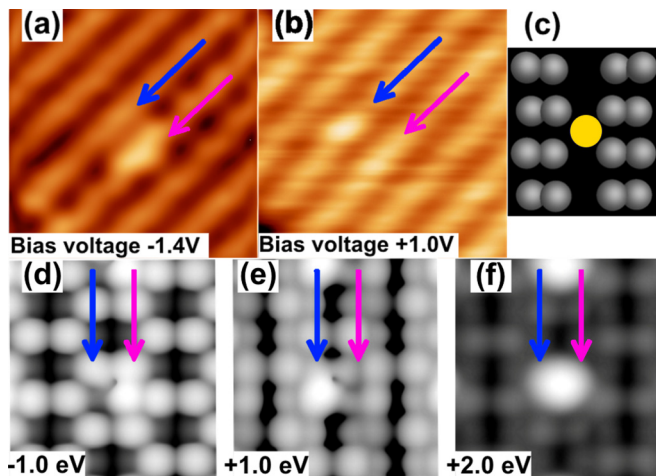


FIG. 9. (Color online) (a) Filled- and (b) empty-state STM images (taken at RT) of the same $5 \times 5 \text{ nm}^2$ region of a Ge(001) surface lightly dosed with Ba; an isolated asymmetric feature [see also Fig. 3(c)] is clearly visible. (c) Scheme indicating the position of the Ba adatom (yellow circle) with respect neighboring Ge surface atoms in the reconstruction (gray circles). Simulated filled- (d) and empty- (e, f) state STM images of the isolated Ba adatom on Ge(001) within the 4×4 unit cell. Pink and blue arrows indicates equivalent Ge dimers rows in the STM and simulated images.

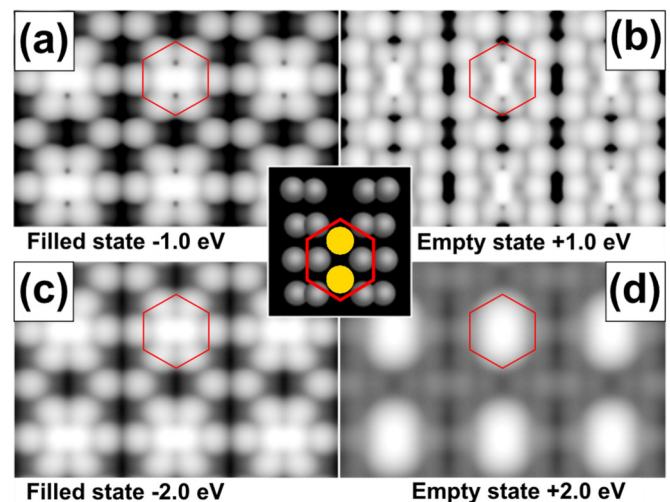


FIG. 10. (Color online) Simulated filled- and empty-state STM images of the isolated Ba dimer on Ge(001) of Fig. 6(k) [six identical (4×4) unit cells reproduced in each image]. Inset in the center, scheme indicating the position of Ba adatoms (yellow circles) with respect to neighboring Ge surface atoms in the reconstruction (gray circles). Red hexagons indicate position of the adsorbed Ba dimers.

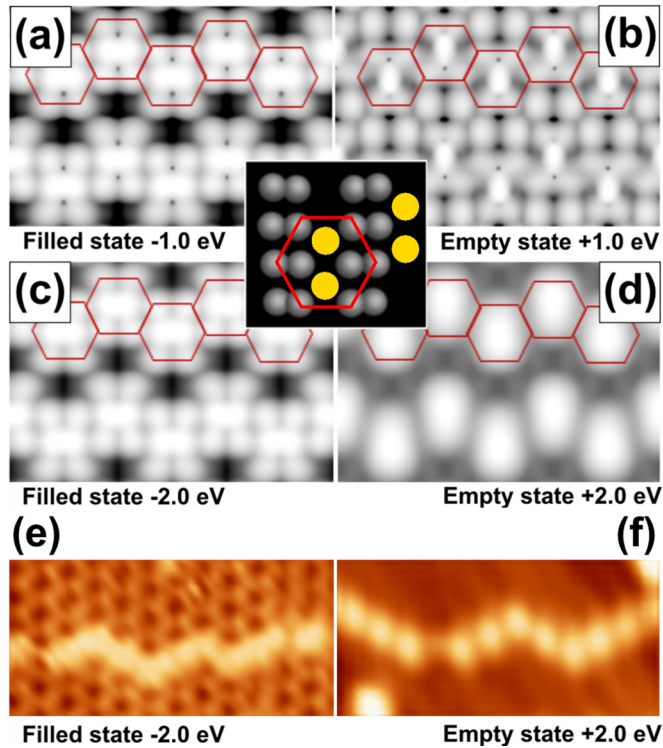


FIG. 11. (Color online) Simulated (a–d) STM images of filled and empty state of the structure of Fig. 7(a), obtained for different values of the integration range [six identical (4×4) unit cells are reproduced in each image]. Inset in the center scheme indicating the position of Ba adatoms (yellow circles) with respect to neighboring Ge surface atoms in the reconstructions (gray balls). Red hexagons indicated position of the adsorbed Ba dimers. (e–f) Representative experimental STM images ($10 \times 5 \text{ nm}^2$) for both bias polarities illustrating the correlation between simulations and experiment.

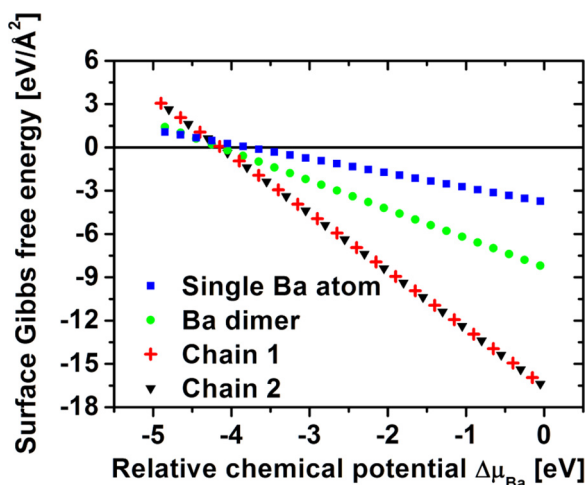


FIG. 12. (Color online) Surface free energy per unit area (vertical axis) as a function of Ba chemical potential (horizontal axis) for Ba-covered Ge(001) surfaces. The most stable configurations are represented by the lines with the lowest (most negative) surface energies. Chains 1 and 2 represent the chain configurations of Figs. 7(a) and 7(b), respectively.

linear, and/or zigzag structures randomly distributed on the surface, which agrees with experiment. Under Ba-poor conditions (large negative Ba chemical potential) isolated Ba dimers are preferred, followed by the less energetically favorable isolated Ba adatoms. This is also consistent with experiment.

IV. COMPARISON WITH THE ALKALI EARTHS ON THE Si(001) SURFACE

In this section we compare the Ba/Si(001), Sr/Si(001), and Ba/Ge(001) systems. There is a clear tendency to form the adatom-induced (Ba, Sr) chains on Si(001), as reported in [35–37]. It has also been shown, however, that the Ba adatoms within the chains on Si(001) could be moved by the STM tip after scanning with positive sample bias only [35]. The latter is inconsistent with the observations reported in this paper for the Ba/Ge(001) system, where Ba adatoms can be moving with both positive and negative sample bias.

Yao *et al.* [38] reported that alkaline-earth elements at low coverage frequently adsorb on the C-type defect on the Si(001) substrate. Similar behavior has not been observed on the Ge(001) substrate, as there is no C defect on that surface. For the nonextended features identified as isolated Ba adatoms on Si(001) at RT that are not absorbed in the vicinity of the C defect [35,38,39], it has been predicted that both the fourfold site in the trough between two Si dimer rows and on top of the dimer row site are preferable for the adatom on Si(001) [40,41]. This is again in contrast to the Ba/Ge(001) system, where the end-dimer bridge site between two Ge dimer rows is clearly preferred for the Ba adatom on Ge(001).

There is also a number of conflicting predictions made for the Ba and/or Sr adatoms on Si(001) that are also inconsistent with the data presented in this paper for the Ba/Ge(001) system. The adatom-induced chains on Si(001) were postulated to be made of single Ba atoms, with each Ba adatom located in the trough between Si dimer rows [35]. This is in contrast to the data reported in this paper. Also Ashman *et al.* [41] in their DFT studies on the Sr/Si(001) system predicted that between 1/6- and 1/4-ML coverage, single and double Sr chains (that consists of Sr dimers, as defined in this paper) will be formed on Si(001). For the Ba/Si(001) system, a number of different atomic chain geometries were predicted using DFT, including those oriented along the Si dimer rows [40].

The claim that the bonding between the Ba adatoms on the Si(001) substrate is mostly covalent in nature [39] has been dismissed in a number of studies (e.g., Refs. [40,41]) for the alkaline-earth metals on Si(001) and is also inconsistent with the data reported in this paper for the Ba/Ge(001) system, where an ionic nature of the bonding between Ba adatoms and the Ge(001) substrate atoms was shown.

V. SUMMARY AND CONCLUSIONS

In this paper the initial stage of Ba adatom adsorption on the Ge(001) surface is studied using STM and DFT. High-resolution, filled- and empty-state STM images for the Ba-adsorbed Ge(001) surfaces with coverages from 0.15 to 1.0 ML, and temperatures between 270 and 770 K were analyzed and compared with density functional theory simulations. Three commonly observed features on Ba-covered

Ge(001) have been identified in the simulated STM images: isolated Ba adatoms (adsorbed at the end-dimer bridge site between the two Ge dimer rows), isolated Ba dimers (adsorbed in the trench between the adjacent Ge dimer rows), and finally, the Ba dimers assembled into chains that run across the substrate dimers. The chains are randomly distributed on the Ge surface and are predominantly arranged in a zigzag pattern. The calculated energetics correctly predict that the formation of chains is preferred at Ba-rich conditions while the formation of isolated Ba dimers is favorable at Ba-poor conditions, consistent with the experimental data. The adsorption of Ba on Ge(001) does not result in any significant bonding rearrangement of the surface Ge dimers, unlike the process of Ba incorporation into Ge(001) described in Ref. [22]. Instead, the adsorption of Ba leads to buckling of the Ge surface dimers by blocking the flip-flop motion of individual Ge atoms, with the Ge dimer bond lengths and angles similar to those of the buckled clean surface. The Ba ad-structures are stabilized mainly by electrostatic interaction between the

positively charged Ba ions and negatively charged dangling bonds of the Ge dimers. The strong ionic character of the Ba-Ge bonds is also manifested by Ba-dimer instabilities within the chains observed during STM imaging for low Ba coverage. Our results are crucial for understanding the on-top Ba adsorption on clean Ge(001), which is believed to be an initial step in the formation of the Ba-based passivation layer on the Ge(001) substrate.

ACKNOWLEDGMENTS

W.K. and N.J.C. acknowledge EPSRC Grant No. EP/I02865X/1. W.K., M.W.R., L.J., and R.C. acknowledge the Polish National Science Center for support (Project No. N-N-202-195840). Innovations for High Performance Microelectronics (IHP GmbH) institute, Frankfurt (Oder), Germany, is acknowledged for support in experimental studies.

W.K. and A.P. contributed equally to this work.

-
- [1] J. A. Kubby, J. E. Griffith, R. S. Becker, and J. S. Vickers, *Phys. Rev. B* **36**, 6079 (1987).
- [2] R. J. Hamers and U. K. Kohler, *J. Vac. Sci. Technol.* **A7**, 2854 (1989).
- [3] M. W. Radny, G. A. Shah, S. R. Schofield, P. V. Smith, and N. J. Curson, *Phys. Rev. Lett.* **100**, 246807 (2008).
- [4] T. Grzela, W. Koczorowski, G. Capellini, R. Czajka, M. W. Radny, N. J. Curson, S. R. Schofield, M. A. Schubert, and T. Schroeder, *J. Appl. Phys.* **115**, 074307 (2014).
- [5] C. Dubourdieu, J. Bruley, T. M. Arruda, A. Posadas, J. Jordan-Sweet, M. M. Frank, E. Cartier, D. J. Frank, S. V. Kalinin, A. A. Demkov, and V. Narayanan, *Nat. Nanotechnol.* **8**, 748 (2013).
- [6] S. Abel, M. Sousa, C. Rossel, D. Caimi, M. D. Rossell, R. Erni, J. Fompeyrine, and C. Marchiori, *Nanotechnology* **24**, 285701 (2013).
- [7] P. Ponath, K. Fredrickson, A. B. Posadas, Y. Ren, X. Wu, R. K. Vasudevan, M. B. Okatan, S. Jesse, T. Aoki, M. R. McCartney, D. J. Smith, S. V. Kalinin, K. Lai, and A. A. Demkov, *Nat. Commun.* **6**, 6067 (2015).
- [8] A. M. Kolpak and S. Ismail-Beigi, *Phys. Rev. B* **85**, 195318 (2012).
- [9] S. Abel, T. Stöferle, Ch. Marchiori, Ch. Rossel, M. D. Rossell, R. Erni, D. Caimi, M. Sousa, A. Chelnokov, B. J. Offrein and J. Fompeyrine, *Nat. Commun.* **4**, 1671 (2013).
- [10] Z. Li, X. Guo, H. B. Lu, Z. Zhang, D. Song, S. Cheng, M. Bosman, J. Zhu, Z. Dong, and W. Zhu, *Adv. Mater.* **26**, 7185 (2014).
- [11] S. Kundu, D. Maurya, M. Clavel, Y. Zhou, N. N. Halder, M. K. Hudait, P. Banerji, and S. Priya, *Sci. Rep.* **5**, 8494 (2015).
- [12] R. A. McKee, F. J. Walker, and M. F. Chisholm, *Phys. Rev. Lett.* **81**, 3014 (1998).
- [13] J. W. Reiner, A. M. Kolpak, Y. Segal, K. F. Garrity, S. Ismail-Beigi, Ch. H. Ahn, and F. J. Walker, *Adv. Mater.* **22**, 2919 (2010).
- [14] R. A. McKee, F. J. Walker, M. B. Nardelli, W. A. Shelton, and G. M. Stocks, *Science* **300**, 1726 (2003).
- [15] K. F. Garrity, M-R. Padmore, Y. Segal, J. W. Reiner, F. J. Walker, Ch. H. Ahn, and S. Ismail-Beigi, *Surf. Sci.* **604**, 857 (2010).
- [16] K. F. Garrity, A. M. Kolpak, and S. Ismail-Beigi, *J. Mater. Sci.* **47**, 7417 (2012).
- [17] R. A. McKee, F. J. Walker, and M. F. Chisholm, *Science* **293**, 468 (2001).
- [18] A. Cattoni, R. Bertacco, M. Riva, M. Cantoni, F. Ciccacci, H. Von Känel, and G. J. Norga, *Mater. Sci. Semicond. Process.* **9**, 701 (2006).
- [19] B. R. Lukanov, J. W. Reiner, F. J. Walker, C. H. Ahn, and E. I. Altman, *Phys. Rev. B* **84**, 075330 (2011).
- [20] B. R. Lukanov, K. F. Garrity, S. Ismail-Beigi, and E. I. Altman, *Phys. Rev. B* **85**, 195316 (2012).
- [21] B. R. Lukanov, K. F. Garrity, S. Ismail-Beigi, and E. I. Altman, *Phys. Rev. B* **89**, 155319 (2014).
- [22] W. Koczorowski, T. Grzela, M. W. Radny, S. R. Schofield, G. Capellini, R. Czajka, T. Schroeder, and N. J. Curson, *Nanotechnology* **26**, 155701 (2015).
- [23] I. Horcas, R. Fernández, J. M. Gómez-Rodríguez, J. Colchero, J. Gómez-Herrero, and A. M. Baro, *Rev. Sci. Instrum.* **78**, 013705 (2007).
- [24] P. E. Blöchl, *Phys. Rev. B* **50**, 17953 (1994).
- [25] J. P. Perdew, J. A. Chevary, S. H. Vosko, K. A. Jackson, M. R. Pederson, D. J. Singh, and C. Fiolhais, *Phys. Rev. B* **46**, 6671 (1992).
- [26] G. Kresse and J. Furthmuller, *Comput. Mater. Sci.* **6**, 15 (1996).
- [27] G. Kresse and J. Furthmuller, *Phys. Rev. B* **54**, 11169 (1996).
- [28] J. Tersoff and D. R. Hamann, *Phys. Rev. Lett.* **50**, 1998 (1983).
- [29] K. Reuter and M. Scheffler, *Phys. Rev. B* **65**, 035406 (2001).
- [30] W.-X. Li, C. Stampfl, and M. Scheffler, *Phys. Rev. B* **68**, 165412 (2003).
- [31] H. J. W. Zandvliet, T. M. Galea, E. Zoethout, and B. Poelsema, *Phys. Rev. Lett.* **84**, 1523 (2000).
- [32] J. M. Carpinelli and B. S. Swartzentruber, *Phys. Rev. B* **58**, R13423(R) (1998).

- [33] Z. C. Dong, T. Yakabe, D. Fujita, and H. Nejoh, *Ultramicroscopy*, **73**, 169 (1998).
- [34] I. A. Suleiman, M. W. Radny, M. J. Gladys, P. V. Smith, J. C. Mackie, E. M. Kennedy, and B. Z. Dlugogorski, *J. Chem. Phys. C* **115**, 13412 (2011).
- [35] X. Hu, X. Yao, C. Peterson, D. Sarid, and Z. Yu, *Surf. Sci.* **445**, 256 (2000).
- [36] R. Bakhtizin, *J. Vac. Sci. Technol. B* **14**, 1000 (1996).
- [37] R. Bakhtizin and J. Kishimoto, *Appl. Surf. Sci.* **95**, 478 (1996).
- [38] X. Yao, X. Hu, D. Sarid, Z. Yu, J. Wang, D. S. Marshall, R. Droopad, J. K. Abrokwah, J. A. Hallmark, and W. J. Ooms, *Phys. Rev. B* **59**, 5115 (1999).
- [39] X. Hu, X. Yao, C. A. Peterson, D. Sarid, Z. Yu, J. Wang, D. S. Marshall, J. A. Curless, J. Ramdani, R. Droopad, J. A. Hallmark, and W. J. Ooms, *Surf. Sci.* **457**, L391 (2000).
- [40] A. J. Ciani, P. Sen, and I. P. Batra, *Phys. Rev. B* **69**, 245308 (2004).
- [41] Ch. R. Ashman, C. J. Forst, K. Schwarz, and P. E. Blochl, *Phys. Rev. B* **69**, 075309 (2004).